INTERNATIONAL JOURNAL OF HEAT AND TECHNOLOGY

ISSN: 0392-8764
Vol. 35, No. 1, March 2017, pp. 91-96
DOI: 10.18280/ijht.350112

A publication of IIETA
International Information and Engineering Technology Association
Advancing the World of Information and Engineering
http://www.iieta.org/Journals/IJHT

Three-dimensional numerical simulation of flow around combined pier based on detached eddy simulation at high Reynolds numbers

Weizheng Cui[1,2], Xiantang Zhang[1*], Zexi Li[1,2], Hui Li[1], Yan Liu[1]

[1]Shandong Provincial Key Laboratory of Civil Engineering Disaster Prevention and Mitigation, Shandong University of Science and Technology, Qingdao 266590, Shandong, P.R. China
[2]College of Civil Engineering and Architecture, Shandong University of Science and Technology, Qingdao 266590, Shandong, P. R. China

Email: zzxhtm@163.com

ABSTRACT

The combined section structure has been extensively used in engineering practice. However, there has been little research on the flow around a combined structure. Based on this situation, the numerical simulations of the flow around a combined pier with Reynolds numbers in the range of 1.0×10^6~2.76×10^6 are performed. The time histories of lift coefficient and drag coefficient of three combined piers with different types (such as combined cylindrical pier, truncated-cone pier, combined truncated-cone pier) in different water depths are analyzed based on detached eddy simulation (DES) by using the fluid dynamics software FLUENT. The results show that the lift coefficient and drag coefficient between the combined cylindrical pier and the truncated-cone pier are basically the same under the condition of the same water depth. When the water depth is 3.0m, the drag coefficient of the combined truncated-cone pier is smaller than that of the combined cylindrical pier and truncated-cone pier. When the water depth is 4.0m or 5.0m, the drag coefficient of the combined truncated-cone pier is greater than that of the combined cylindrical pier and the truncated-cone pier. The form of the cross section of the submerged portion of the combined pier has a significant influence on the average drag coefficient under the condition of a different water depth.

Keywords: High Reynolds Numbers, Combined Pier, Drag Coefficient, Lift Coefficient.

1. INTRODUCTION

The flow around a cylinder at high Reynolds numbers is turbulence that can be compressed. Turbulence is an extraordinarily complex three-dimensional flow, which is unsteady, erratic and composed of eddies. The characteristic of turbulence is the fluctuation of physical quantity generated by a random motion of vortex at different scales [1]. The numerical simulation of turbulence can be investigated by using Direct-Numerical Simulation(DNS), Reynolds-Averaged Navier-Stokes(RANS), Large-Eddy Simulation(LES), and Detached-Eddy Simulation(DES). RANS has been used for the average processing to the Navier-Stokes equation in time. The equation after time-averaged processing is solved and the turbulence pulsation of the fluid is ignored, which makes it difficult to capture the instantaneous pulsation of the fluid [2]. Some promising results of large-eddy simulations(LES) have been reported by Breuer [3, 4] on a cylinder in a uniform cross-flow($Re=3.9\times10^3$ and 1.4×10^5, respectively), but an unavoidable problem in the use of LES is the enormous computational cost required to sufficiently resolve the near-wall region, especially in high-Re cases. A possible alternative for LES is the detached-eddy simulation(DES), which is one of the hybrid methods that combines URANS and LES to obtain realistic solutions of practical high-Re flows at acceptable computational costs [5-7]. Travin et al. [8] performed the DES of flow around a cylinder in a uniform cross-flow in the subcritical(laminar-separation) and postcritical(turbulent-separation) flow regimes. The results were very similar to those of the experiment and also with LES, especially at a subcritical Reynolds number of 5.0×10^4. Gu et al. [9] applied DES to study the flow characteristics of the Tension-Leg Platform under a uniform current, and discussed the drag coefficient, lift coefficient and its power spectrum, pressure coefficient and vortex behind Tension-Leg Platform. The results of their study showed some periodicity and "beating" behavior of drag coefficient and lift coefficient. Chang et al. [10] used the DES method based on the SST two-equation turbulence model to stimulate the incompressible viscous flow around a cylinder. They proved that the DES method is valid and reliable to simulate the flow around a cylinder with a low or higher subcritical Reynolds number. Xu et al. [11] investigated the separated turbulent flow around a cylinder using LES, DES, and URANS, who asserted that the DES-based Spalart-Allmaras and k-ωShear-Stress-Transport models in DES can be reasonably calculated for most simulations. Nishino et al. Reference [12] utilized URANS and DES to perform flow

around a cylinder. They discovered that DES can precisely capture the intermittence of the vortex shedding in the near-wake region.

As mentioned above, most of the current and recent research has focused on flow around a single cross section cylinder, while the flow around the combined section structure, such as the combined pier, is seldom involved. The combined section is used in many important harbors, coastal and offshore engineering designs, such as deep-sea drilling platform, wading bridge, and port and dock. Figure 1 shows some common forms of combined bridge piers [13, 14]. Thus, it is of great theoretical and practical significance to study the flow around the combined pier.

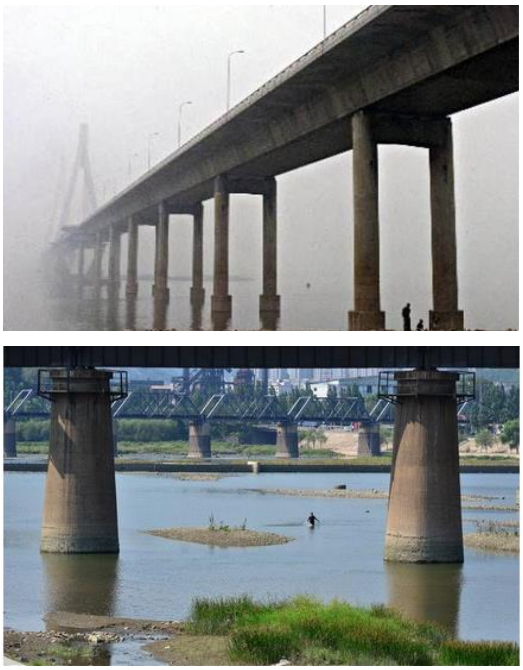

Figure 1. Combined bridge piers

2. CREATION OF NUMERICAL MODEL

Two kinds of combined piers(combined cylindrical pier and truncated-cone pier), which are frequently adopted in actual engineering, are chosen to establish three-dimensional numerical models for different types of combined piers at high Reynolds numbers. Furthermore, in order to study the variation laws of lift and drag coefficients of flow around a combined section, the third combined pier(combined truncated-cone pier) is assumed based on these two kinds of combined piers. Three kinds of combined piers are shown in Figure 2.

Nine different cases are considered. Each case is named according to the kind of combined piers column and the simulated water depth. To simplify the presentation, A, B, C respectively expresses a combined cylindrical pier, a truncated-cone pier and a combined truncated-cone pier. For example, A/E(3.0) stands for the numerical simulation of a combined cylindrical pier in a water depth of 3.0m. The FLUENT is used to establish the three-dimensional numerical models. The transient rheology is solved by a pressure solver. The governing equation is discretized by the finite volume method. The pressure equation is discretized with second order accuracy [15, 16]. The three-dimensional computation domain is shown in Figure 3.

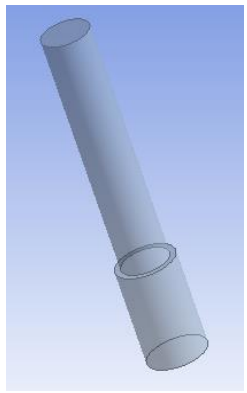

(A) Combined cylindrical pier

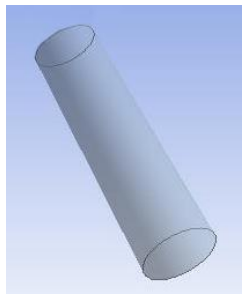

(B) Truncated-cone pier

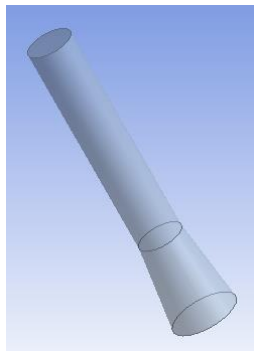

(C) Combined truncated-cone Pier

Figure 2. Three combined piers with different types

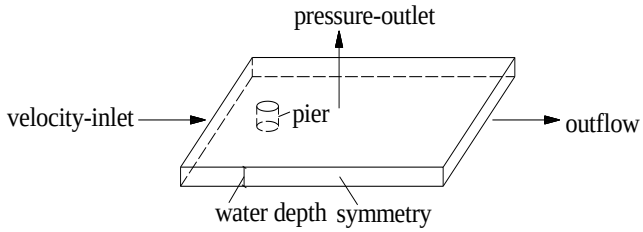

Figure 3. Three-dimensional computational domain

The left boundary of computational domain is defined as a velocity inlet boundary. The velocity is 0.4m/s, and the direction of velocity is perpendicular to the inlet boundary. In this paper mainly studies the turbulent flow around a combined pier. The turbulent intensity I and hydraulic diameter D are specified in the turbulence method. I can be estimated by the empirical formula:

$$I = 0.16 \times (\mathrm{Re})^{-1/8} \quad (1)$$

where, Re represents the Reynolds number. The structural sizes and related parameters of cases are shown in Table 1.

Table 1. The structural sizes and related parameters of cases

CASE	Lower portion of pier			Upper portion of pier			Hydraulic diameter D (m)	Re ($\times 10^6$)	Turbulence intensity I (%)
	Shape	Bottom diameter D_u (m)	Height H (m)	Shape	Bottom diameter D_u (m)	Height H (m)			
A/E(3.0)	cylinder	2.5	4.0	cylinder	2	10	2.50	1.00	2.8
B/E(3.0)	truncated-cone	2.5	8.3	-	-	-	6.64	2.64	2.5
C/E(3.0)	truncated-cone	3.0	4.0	cylinder	2	10	6.40	2.55	2.5
A/E(4.0)	cylinder	2.5	4.0	cylinder	2	10	2.50	1.00	2.8
B/E(4.0)	truncated-cone	2.5	8.3	-	-	-	6.72	2.68	2.5
C/E(4.0)	truncated-cone	3.0	4.0	cylinder	2	10	6.37	2.54	2.5
A/E(5.0)	cylinder	2.5	4.0	cylinder	2	10	6.93	2.76	2.6
B/E(5.0)	truncated-cone	2.5	8.3	-	-	-	6.42	2.56	2.5
C/E(5.0)	truncated-cone	3.0	4.0	cylinder	2	10	6.60	2.63	2.5

The upper boundary of the computational domain is defined as a pressure outlet boundary maintained as the atmospheric pressure. The right boundary is defined as the outflow boundary. Both sides are defined as symmetry boundaries. The bottom boundary and the surface of the combined pier are set as the wall boundary.

3. GOVERNING EQUATION

The governing equations are the three-dimensional compressible Navier-Stokes(N-S) equations. The equations in the LES are the Favre-filtered three-dimensional compressible N-S equations, which can be written in terms of generalized coordinates(ξ, η, ζ) as in Ref. [11].

$$\frac{\partial}{\partial t}\left(\frac{Q}{J}\right)+\frac{\partial(F-F_V)}{\partial \xi}+\frac{\partial(G-G_V)}{\partial \eta}+\frac{\partial(H-H_V)}{\partial \zeta}=0 \tag{2}$$

where, J is the transformation Jacobian, Q is the vector of variables, F, G and H are the convective flux terms, F_V, G_V and H_V are the viscous flux terms. For the sake of clarity, the detailed formulations of these terms are not shown here and can be found in Ref. [17].

RANS equations can be obtained by applying the ensemble average to the N-S equations. The formulations in the RANS or URANS are similar to Eq.(2) used in LES, but the mean quantities denote the ensemble average or the Reynolds average[11].

To obtain the DES-SA formulation and the DES-SST formulation, the distance to the closest wall d in the S-A model and the length scale L_t in the SST model can be modified as follows [18, 19].

$$\tilde{d} = \min(d, C_{DES}\Delta) \tag{3}$$

$$\tilde{L}_t = \min(L_t, C_{DES}\Delta) \tag{4}$$

where, Δ is the largest distance between the cell centers. C_{DES} is a constant and commonly is taken as 0.65 in Eq.(3), but C_{DES} represents another constant in Eq.(4).

The zonal hybrid RANS/LES approach is also employed by combining the SST model and the one-equation SGS eddy viscosity model proposed by Yoshizawa [20]. This zonal hybrid RANS/LES method acts as the RANS in the detached flow region and as the LES in the separated flow region[11].

4. CHECKING CALCULATION OF NUMERICAL MODEL

In order to ensure the accuracy of the calculation results, the authors firstly checked the model and simulation method. The model with Re=1.4×10^5 is established, and the column diameter is 0.3m, the fluid velocity 0.47m/s, the water depth 3.0m. Deng et al. [21] separated the vortex motion in the flow by DES and pointed out that the fluctuation of time histories of the lift and drag coefficients is of significant randomness, and it is necessary to simulate a sufficiently long flow time in order to obtain a stable time average. Thus, statistics are started from t=80s. The time histories of the lift coefficient and drag coefficient of the checking model are shown in Figure 4.

The lift coefficient and drag coefficient are important parameters to describe the flow around a cylinder. Lift and drag coefficients are defined as:

$$C_L = \frac{F_L}{\frac{1}{2}\rho S v^2} \tag{5}$$

$$C_D = \frac{F_D}{\frac{1}{2}\rho S v^2} \tag{6}$$

where, F_L and F_D are the lift force and the drag force of the pier, respectively; ρ is the fluid density; v denotes the velocity of fluid flow at infinity; S is defined as the effective section area perpendicular to the flow direction $S=D_0 l$; D_0 is the pier diameter of the checking model and l is the submerged depth of the pier.

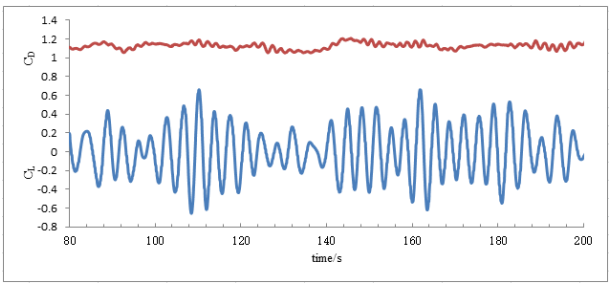

Figure 4. The time histories of lift coefficient and drag coefficient of checking model

It can be seen from Figure 3 that the fluctuant cycles of the checking model are irregular and the amplitudes are random. Additionally, the oscillation frequency of the drag coefficient is about twice that of the lift coefficient in the process of vortex shedding. This can be explained by the reason that the shedding of the upper and lower vortices causes the drag force to change once, and these two vortices affect the change in the lift force. The trends of the lift and drag coefficients agree well with the numerical simulation calculation results made by Hao et al. [22], but there is a large deviation in value. This may be caused by different methods of simulation and/or other reasons.

The weighted average of the drag coefficient is calculated. There is a large deviation between the numerical results of this study and the simulation results of Breuer [4], and the maximum value is 12%. This may be caused by the difference in the number of grid or parameter settings and/or other reasons. However, the results of the study agree well with the experimental results of Refs. [23, 24], and the maximum deviation is less than 9%.

5. THE ANALYSIS OF NUMERICAL RESULTS

The lift coefficients and drag coefficients of nine cases are calculated and analyzed. Water is selected as the fluid medium in this paper. The original variables are used, rather than non-dimensional values. The time histories of the lift coefficient and drag coefficient of each of the nine cases are shown in Figure 5. The average drag coefficients of the nine cases are shown in Table 2.

Compared with the flow around a cylindrical pier with $Re=1.4\times10^5$, the oscillation amplitudes of lift coefficients and drag coefficients of the flow around the combined piers with Reynolds numbers in the range of 1.0×10^6~2.76×10^6 are clearly reduced, and fluctuations no longer show periodic variations, as indicated in Figure 5. The time to reach stability of calculation is clearly lagging behind when the water depth increases from 3.0m to 5.0m. When the water depth is 3.0m or 4.0m for combined truncated-cone pier, the time when the drag coefficient reaches a stable state later than that of the combined cylindrical pier and truncated-cone pier. When the water depth is 5.0m, compared with other two cases, the time of the drag coefficient of a combined cylindrical pier ultimately reaches stability of calculation.

As can be seen from Figure 5(a), after reaching stability of calculation, lift coefficients and drag coefficients of case A/E(3.0) and case B/E(3.0) are basically the same at a depth of 3.0m, while the drag coefficient of case C/E(3.0) is smaller and the lift coefficient is larger. When the water depth is 4.0m, the drag coefficient of case C/E(4.0) is significantly greater than that of case A/E(4.0) and case B/E(4.0), and its value reaches 0.4565. The drag coefficient of case B/E(4.0) is the smallest, at only about 0.3902. The lift coefficients of these three cases are basically the same, as presented in Figure 5(b). With the increase of water depth to 5.0m, the states of lift coefficients of case A/E(5.0), case B/E(5.0) and case C/E(5.0) are in disorder and the fluctuations increase. Drag coefficients of case A/E(5.0) and case B/E(5.0) are basically consistent, and the drag coefficient of case C/E(5.0) is greater than that of case A/E(5.0) and case B/E(5.0), as shown in Figure 5(c). From what has been discussed above, the lift coefficients and drag coefficients between the combined cylindrical pier and the truncated-cone pier are basically the same under the condition of the same water depth. Additionally, when the water depth is 3.0m, the drag coefficient of the combined truncated-cone pier is smaller than that of the combined cylindrical pier and the truncated-cone pier. When the water depth is 4.0m or 5.0m, the drag coefficient of the combined truncated-cone pier is greater than that of the combined cylindrical pier and the truncated-cone pier.

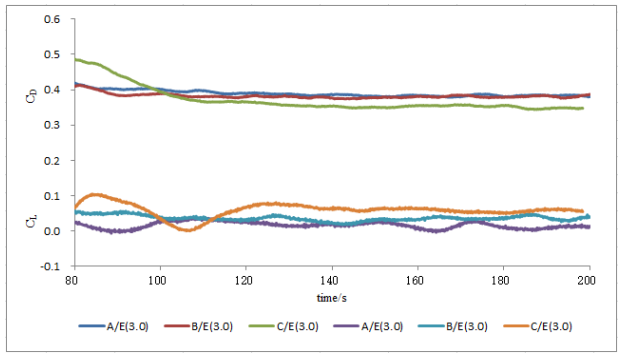

(a)The water depth is 3.0m

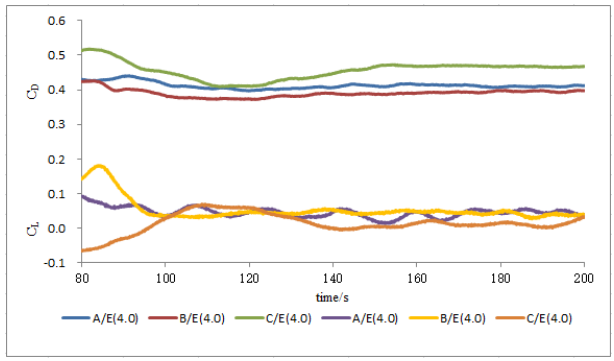

(b)The water depth is 4.0m

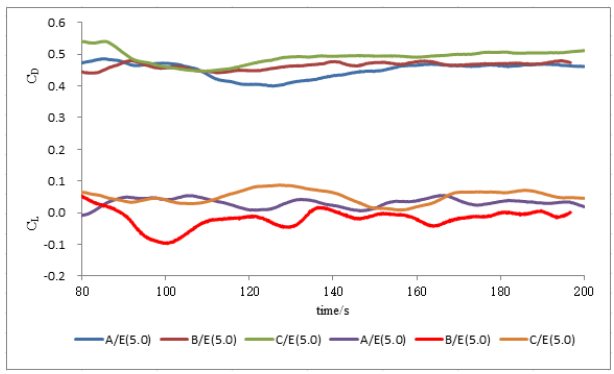

(c)The water depth is 5.0m

Figure 5. The time histories of lift coefficients and drag coefficients of computational models(a),(b),(c)

Table 2. The average drag coefficient of nine cases

CASE	A/E (3.0)	B/E (3.0)	C/E (3.0)	A/E (4.0)	B/E (4.0)
C_D	0.3845	0.38	0.3533	0.4115	0.3948
CASE	C/E (4.0)	A/E (5.0)	B/E (5.0)	C/E (5.0)	
C_D	0.4681	0.4654	0.4715	0.5026	

The average drag coefficients under various cases are shown in Table 2. It is obvious from the table that the deviation of the average drag coefficients between case A/E(3.0) and case A/E(4.0) is about 7%, while the deviation between case A/E(4.0) and case A/E(5.0) is 13%. It can be seen that the deviation of average drag coefficients between case B/E(3.0) and case B/E(4.0) is about 4%, whereas the deviation between case B/E(4.0) and case B/E(5.0) is 19%. The deviation of the average drag coefficient between case C/E(3.0) and case C/E(4.0) is about 32%, while the deviation between case C/E(4.0) and case C/E(5.0) is 4%. Based on this table, the authors believe that the form of cross section of the submerged portion of the combined pier has a significant influence on the calculation of the average drag coefficient under the condition of a different water depth.

In this study, the average drag coefficients of case A/E(3.0) and case A/E(4.0) with the same Reynolds number ($Re=1.0\times10^6$) are in conformitywith Refs. [25, 26] and experimental results in Ref. [27], which can verify the accuracy of the calculation model. Compared with the checking model, the average drag coefficients of these two cases are clearly reduced, which can be explained by the reason that the flow in the boundary layer changes from laminar to turbulent in the vicinity of $Re=3.0\times10^5$. The friction drag of the turbulent boundary layer is larger than that of the laminar boundary layer. However, turbulence separates from the surface later, which forms a small wake area. The drag force of the flow around a blunt body is mainly pressure resistance, so the total drag force decreased significantly. In addition, the deviation of average drag coefficients between these two cases is about 7%, which shows that the different number of grids has an impact on the calculation of the average drag coefficient.

6. CONCLUSIONS

The numerical model of $Re=1.4\times10^5$ is compared with several previous studies to verify the accuracy of the calculation model and simulation method. The numerical analysis of lift and drag coefficients of combined piers in different water depths are carried out, and some typical conclusions are obtained. The lift coefficients and drag coefficients between the combined cylindrical pier and the truncated-cone pier are basically the same under the condition of same water depth. When the water depth is 3.0m, the drag coefficient of the combined truncated-cone pier is smaller than that of the combined cylindrical pier and the truncated-cone pier. The drag coefficient of the combined truncated-cone pier is greater than that of the combined cylindrical pier and the truncated-cone pier when the water depth is 4.0m or 5.0m. The form of cross section of the submerged portion of the combined pier has a great influence on the calculation of the average drag coefficient under the condition of different water depths. The number of grids will influence the average drag coefficient of flow around the cylindrical structure in the numerical simulation.

ACKNOWLEDGMENT

This work is financed and supported by Shandong Provincial Natural Science Foundation China (ZR2013EEM023), the Project of Shandong Province Higher Educational Science and Technology Program (J13LG05, J14LG06), the Promotive Research Fund for Young and Middle-aged Scientists of Shandong Province (BS2015HZ017), the Scientific Research Foundation of Shandong University of Science and Technology for Recruited Talents (2014RCJJ043), the Project of Shandong University of Science and Technology Graduate Innovation Fund (SDKDYC170213).

REFERENCES

[1] Zhao M., Mao J., Xi Y.H. (2015). Research on drag characteristic of flow around finite circular cylinder at high Reynolds numbers, *Journal of Mechanical Engineering*, Vol. 51, No. 22, pp. 176-182. DOI: 10.3901/JME.2015.22.176 (in Chinese)

[2] Zhao W.W., Wan D.C. (2016). Numerical study of 3D flow past a circular cylinder at subcritical Reynolds number using SST-DES and SST-URANS, *Chinese Journal of Hydrodynamics*, Vol. 31, No. 1, pp. 1-8. DOI: 10.16076/j.cnki.cjhd.2016.01.001 (in Chinese)

[3] Breuer M. (1999). Numerical and modeling influences on large eddy simulations for the flow past a circular cylinder, *International Journal of Heat and Fluid Flow*, Vol. 19, No. 5, pp. 512–521, Oct., 1998. DOI: 10.1016/S0142-727X(98)10015-2

[4] Breuer M. (2000). A challenging test case for large eddy simulation: high Reynolds number circular cylinder flow, *International Journal of Heat and Fluid Flow*, Vol. 21, No. 21, pp. 648-654. DOI: 10.1016/S0142-727X(00)0 0056-4

[5] Shur M., Spalart P.R., Strelets M., Travin A. (1999). Detached-eddy simulation of an airfoil at high angle of attack, *Engineering Turbulence Modelling and Experiments*, Vol. 4, pp. 669–678. DOI: 10.1016/B978-008043328-8/50064-3

[6] Breuer M., Jovičić N., Mazaev K. (2003). Comparison of DES, RANS and LES for the separated flow around a flat plate at high incidence, *International Journal of Numerical Methods in Fluids*, Vol. 41, No. 4, pp. 357–388. DOI: 10.1002/fld.445

[7] Squires K.D. (2004). Detached-eddy simulation: current status and perspectives, *Springer Netherlands*, Vol. 9, pp. 465–480.

[8] Travin A., Shur M., Strelets M., Spalart P. (2000). Detached-eddy simulations past a circular cylinder, *Flow, Turbulence and Combustion*, Vol. 63, No. 1, pp. 293–313. DOI: 10.1023/A:1009901401183

[9] Gu J.Y., Huang X.H., Lu Y.X. (2015). Study on the hydrodynamic characteristics of TLP's main hull based on DES method, *Journal of Ship Mechanics*, Vol. 19, No. 1-2, pp. 52-15. (in Chinese)

[10] Chang S.P., Wang Y.S., Pang Z.Y. (2009). Numerical simulation of flow around circular cylinder using SST DES model, *Ship Science and Technology*, Vol. 31,

No. 2, pp. 30-33. DOI: 10.3404/j.issn.1672-7649.2009.02.003 (in Chinese)
[11] Xu C.Y., Chen L.W., Lu X.Y. (2007). Large-eddy and detached-eddy simulations of the separated flow around a circular cylinder, *Journal of Hydrodynamics. Ser. B*, Vol. 19, No. 5, pp. 559-563. DOI: 10.1016/S1001-6058(07)60153-X
[12] Nishino T., Roberts G. T., Zhang X. (2008). Unsteady RANS and detached-eddy simulations of flow around a circular cylinder in ground effect, *Journal of Fluids and Structures*, Vol. 24, No. 1, pp. 18-33. DOI: 10.1016/j.jfluidstructs.2007.06.002
[13] http://blog.sina.com.cn/s/blog_70c59c780100nv39.html.
[14] http://www.huitu.com/photo/show/20140831/222004521347.html.
[15] Zhang X.T., Chen X.J., Huang J.M., Zhou H.M., Wang Q. (2015). Optimum design of bridge cross section with low clearance considering wave load effects based on numerical wave-tank, *Journal of Coastal Research*, No. 73, pp. 232-237. DOI: 10.2112/SI73-041.1
[16] Zhang X.T., Zhou H.M., Wang H.L., Gao K.N. (2012). Analysis on wave forces acting on box girder of twin-decks offshore bridge, *Przeglad Elektrotechniczny*, Vol. 88, No. 9, pp. 29-32.
[17] Lu X., Wang S., Sung H.G., Hsieh S.Y., Yang V. (2005). Large eddy simulations of turbulent swirling flows injected into a dump chamber, *Journal of Fluid Mechanics*, Vol. 527, No. 527, pp. 171-195. DOI: 10.1017/S0022112004002927
[18] Spalart P., Allmaras S. (1992). A one-equation turbulence model for aerodynamic flows, *La Recherche Aerospatiale*, Vol. 439, No.1, pp. 5-21. DOI: 10.2514/6.1992-439
[19] Menter F. (1992). Improved two-equation k turbulence models for aerodynamic flows, *NASA TM 103975*, 1992.
[20] Yoshizawa A., Horiuti K. (1985). A statistically-derived subgrid-scale kinetic energy model for large-eddy simulation of turbulent flows, *Journal of the Physical Society of Japan*, Vol. 54, No. 8, pp. 2834-2839. DOI: 10.1143/JPSJ.54.2834
[21] Deng F., Wu Y.Z., Liu X.Q. (2008). Simulation of vortex in separated flows with DES, *Chinese Journal of Computational Physics*, Vol. 25, No. 6, pp. 683-688. (in Chinese)
[22] Hao P., Li G.D., Yang L., Chen G. (2012). Large eddy simulation of the circular cylinder flow in different regimes, *Chinese Journal of Applied Mechanics*, Vol. 29, No. 4, pp. 437-445. (in Chinese)
[23] Zdravkovich M.M. (1997). Flow around circular cylinders: fundamentals, 1st Ed., Oxford University Press, New York, pp. 305-388.
[24] Cantwell B., Coles D. (1983). An experimental study of entrainment and transport in the turbulent near wake of a circular cylinder, *Journal of Fluid Mechanics*, Vol. 139, pp. 321-374. DOI: 10.1017/S0022112083002189
[25] Schlichting H. (1988). *Boundary-layer Theory*, 7th Edition, Science Press, Beijing, pp. 130-193.
[26] Schliching H. (1979). *Boundary-layer Theory*, McGraw-Hill Book Company, New York, pp. 112-203.
[27] Franke J., Frank W. (2002). Large eddy simulation of the flow past a circular cylinder at Re D=3900, *Journal of Wind Engineering and Industrial Aerodynamics*, Vol. 90, No. 10, pp. 1191-1206.

NOMENCLATURE

I	turbulent intensity
D	hydraulic diameter
Re	Reynolds number
d	undetermined fitting coefficient
J	transformation Jacobian
Q	vector of variables
F	convective flux terms
G	convective flux terms
H	convective flux terms
F_V	viscous flux terms
G_V	viscous flux terms
H_V	viscous flux terms
d	the distance to the closest wall in the S-A model
L_t	the length scale in the SST model
Δ	largest distance between the cell centers
C_{DES}	constant
t	time
F_L	lift force of the pier
F_D	drag force of the pier
ρ	fluid density
v	velocity of fluid flow at infinity
S	effective section area perpendicular to the flow direction
D_0	pier diameter of the checking model
L	submerged depth of the pier
C_D	drag coefficient
C_L	lift coefficient
D_u	diameter of the combined pier

Subscripts

V	symbol of viscous flux terms
t	symbol of length scale in the SST model
DES	symbol of DES model
L	symbol of lift force
D	symbol of drag force
0	symbol of pier diameter of the checking model
u	symbol of diameter of combined pier